

RESEARCH ARTICLE | APRIL 25 2023

Deep UV transparent conductive Si-doped Ga₂O₃ thin films grown on Al₂O₃ substrates

Zhenni Yang; Xiangyu Xu; Yan Wang; ... et. al



Appl. Phys. Lett. 122, 172102 (2023)

<https://doi.org/10.1063/5.0147004>



CrossMark

Time to get excited.
Lock-in Amplifiers – from DC to 8.5 GHz

[Find out more](#)

Deep UV transparent conductive Si-doped Ga₂O₃ thin films grown on Al₂O₃ substrates

Cite as: Appl. Phys. Lett. **122**, 172102 (2023); doi: [10.1063/5.0147004](https://doi.org/10.1063/5.0147004)

Submitted: 18 February 2023 · Accepted: 12 April 2023 ·

Published Online: 25 April 2023



View Online



Export Citation



CrossMark

Zheni Yang,^{1,2} Xiangyu Xu,¹ Yan Wang,¹ Siliang Kuang,^{1,2} Duanyang Chen,^{3,4} Hongji Qi,^{2,3,4,a)} and K. H. L. Zhang^{1,a)}

AFFILIATIONS

¹State Key Laboratory of Physical Chemistry of Solid Surfaces, College of Chemistry and Chemical Engineering, Xiamen University, Xiamen 361005, People's Republic of China

²Hangzhou Institute of Optics and Fine Mechanics, Hangzhou 311421, China

³Key Laboratory of Materials for High Power Laser, Shanghai Institute of Optics and Fine Mechanics, Chinese Academy of Sciences, Shanghai 201800, China

⁴Research Center of Laser Crystal, Shanghai Institute of Optics and Fine Mechanics, Chinese Academy of Sciences, Shanghai 201800, China

^{a)}Authors to whom correspondence should be addressed: qhj@siom.ac.cn and Kelvinzhang@xmu.edu.cn

ABSTRACT

β -Ga₂O₃ is attracting considerable attention for applications in power electronics and deep ultraviolet (DUV) optoelectronics owing to the ultra-wide bandgap of 4.85 eV and amendable *n*-type conductivity. In this work, we report the achievement of Si-doped β -Ga₂O₃ (Si: β -Ga₂O₃) thin films grown on vicinal α -Al₂O₃ (0001) substrates with high electrical conductivity and DUV transparency of promising potential as transparent electrodes. The use of Al₂O₃ substrates with miscut angles promotes step-flow growth mode, leading to substantial improvement of crystalline quality and electrical properties of the Si: β -Ga₂O₃ films. A high conductivity of 37 S·cm⁻¹ and average DUV transparency of 85% have been achieved for 0.5% Si-doped film grown on a 6° miscut substrate. High-resolution x-ray and ultraviolet photoemission spectroscopy were further used to elucidate the surface electronic properties of the grown Si: β -Ga₂O₃ films. An upward surface band bending was found at the surface region of Si: β -Ga₂O₃ films. Interestingly, all the Si: β -Ga₂O₃ films have a very low work function of approximately 3.3 eV, which makes Si: β -Ga₂O₃ suitable materials for efficient electron injection. The present Si: β -Ga₂O₃ films with high conductivity, DUV transparency, and low work function would be useful as the DUV transparent electrode to develop advanced DUV optoelectronic devices.

Published under an exclusive license by AIP Publishing. <https://doi.org/10.1063/5.0147004>

Deep ultraviolet (DUV, ~200–300 nm) transparent oxide semiconductors (TCOs) have been actively developed as transparent electrodes for DUV optoelectronic devices, such as laser diodes (LDs), DUV light emitting diodes (LEDs), and solar-blind photodetectors.^{1–4} DUV LEDs and LDs have widely been applied in coronavirus sterilization, water/air purification, biochemistry, curing, printing, sensor, and optical data storage.^{5–7} However, conventional TCOs, like Sn-doped In₂O₃ (ITO), F-doped SnO₂ (FTO), and Al-doped ZnO (AZO), abruptly lost high transmittance in the UV region because of their small bandgaps of less than 3.5 eV. The non-availability of DUV transparent electrodes results in DUV LEDs with an external quantum efficiency as low as about 1%.⁸

Ga₂O₃ (all the Ga₂O₃ discussed in the following are β -Ga₂O₃ phases unless otherwise specified) is an emerging ultra-wide bandgap

semiconductor, and its bandgap of ~4.8 eV makes it a natural advance in the field of DUV optoelectronic devices. The *n*-type doping Ga₂O₃ using group IV elements, such as Si, Ge, and Sn, can achieve a wide range of carrier concentrations from 10¹⁵ to 10²⁰ cm⁻³.^{9–11} Among them, degenerately doped Ga₂O₃ is regarded as a promising candidate for DUV transparent electrodes because it maintains both DUV transmittance and electrical conductivity. Recently, we have reported the homoepitaxial growth of Si-doped Ga₂O₃ (Si:Ga₂O₃) thin films on semi-insulating Fe-doped Ga₂O₃ substrates using pulsed laser deposition (PLD), which exhibits a record-high conductivity of 2500 S·cm⁻¹ and ~65% transparency at a wavelength of 300 nm.¹² Si is considered as an efficient dopant because the weak hybridization between Si 3s and Ga 4s orbital can maintain the low effective mass and the high electron mobility of Si:Ga₂O₃ thin films.¹³ Despite these

excellent electrical properties, the cost, wafer size, and low thermal conductivity of Ga_2O_3 substrates limit the $\text{Si}:\text{Ga}_2\text{O}_3$ films as transparent electrodes for further applications at the present stage.^{14,15}

$\alpha\text{-Al}_2\text{O}_3$ (simplified as Al_2O_3) has widely been used in current process systems of GaN-based and AlGaIn-based DUV LEDs due to its technical maturity, low cost, and availability of large-size substrates.^{16,17} Furthermore, Al_2O_3 has an ultra-large bandgap of 8.8 eV, which warrants high transparency over a wide range in the DUV spectrum. Therefore, growth of $\text{Si}:\text{Ga}_2\text{O}_3$ films on Al_2O_3 substrates is a viable strategy to exploit the potential of $\text{Si}:\text{Ga}_2\text{O}_3$ as DUV transparent and conductive films. It is worth mentioning that the large lattice mismatch and different crystal symmetry between Ga_2O_3 and Al_2O_3 pose a challenge to the growth of high-quality Ga_2O_3 thin films on Al_2O_3 .^{18,19} Previous works showed that Si- and Sn-doped Ga_2O_3 thin films grown on Al_2O_3 substrates possess low electrical conductivity of $< 8 \text{ S}\cdot\text{cm}^{-1}$.^{20–22} Recently, Rafique *et al.* reported that the use of vicinal Al_2O_3 (0001) substrates with appropriate miscut angles can promote step-flow growth mode and then reduce twin lamellae and stacking mismatch boundaries in the grown Ga_2O_3 films.²³ A high mobility of $106.6 \text{ cm}^2 \text{ V}^{-1} \text{ s}^{-1}$ was achieved due to the substantially improved crystalline quality. The enhancement of crystallinity and modulation of the domain structure for films were also demonstrated by previous studies.^{24–26} However, films prepared by Rafique *et al.* exhibited a low conductivity of $\sim 8 \text{ S}\cdot\text{cm}^{-1}$, because of a low carrier concentration in undoped Ga_2O_3 . Si or Sn doping would be an effective way to further enhance electrical conductivity. In addition, the vicinal substrates were employed to improve the performance of solar-blind photodetectors and LEDs.^{27–29}

In this work, we report the use of vicinal Al_2O_3 (0001) substrates to grow $\text{Si}:\text{Ga}_2\text{O}_3$ thin films. By optimizing Si doping level and substrate miscut angles, $\text{Si}:\text{Ga}_2\text{O}_3$ films with a high conductivity of $37 \text{ S}\cdot\text{cm}^{-1}$ and average transparency (260–400 nm) over 85% have been achieved. The surface electronic structures of the $\text{Si}:\text{Ga}_2\text{O}_3$ films are analyzed in detail by high-resolution photoemission spectroscopy and discussed in terms of device applications.

The Si-doped Ga_2O_3 films were grown on Al_2O_3 (0001) substrates with different miscut angles (0° , 2° , and 6°) toward the $[11\bar{2}0]$ direction using PLD from homemade targets. The targets were obtained by mixing and grinding the appropriate proportions [i.e., Si/(Si + Ga)] of Ga_2O_3 (99.999%) and SiO_2 (99.999%) polycrystalline powder. XRD θ - 2θ scans and phi scans were performed by Rigaku SmartLab XRD system with Cu $K\alpha$ radiation. The carrier concentration and electron mobility were measured by Hall measurement with a direct current (DC) bias using the four-point van der Pauw configuration at room temperature. The 5 nm Ni/50 nm Au top electrodes were deposited on the corners of the films by magnetron sputtering to achieve Ohmic contacts. The x-ray photoelectron spectroscopy (XPS, Al $K\alpha_1$, $h\nu = 1486.6 \text{ eV}$) and ultraviolet photoemission spectroscopy (UPS, He I, $h\nu = 21.22 \text{ eV}$) were performed by Thermo Scientific ESCALAB Xi⁺ at a 90° takeoff angle. The binding energy was calibrated by setting the Au $4f_{7/2}$ peak of Au foil placed in the electrical contact with the film surface at binding energy of 84.0 eV.

A series of growth parameters (e.g., Si doping concentration, temperatures, and oxygen pressures) for $\text{Si}:\text{Ga}_2\text{O}_3$ thin films were investigated to optimize the crystal structure and electrical properties of Ga_2O_3 (Fig. S1). Among all films grown on Al_2O_3 (0001) substrate without miscut angle, the 0.5% Si-doped film grown at 600°C in O_2

pressure of 1 Pa shows the best electrical properties with the mobility of $2.5 \text{ cm}^2 \text{ V}^{-1} \text{ s}^{-1}$. Subsequently, vicinal substrates with different miscut angles (δ) of 2° and 6° toward the $[11\bar{2}0]$ direction were used to further improve the crystal quality. Figure 1(a) shows the θ - 2θ XRD patterns for $\sim 500 \text{ nm}$ thick 0.5% Si-doped films grown on Al_2O_3 substrates without miscut angle ($\delta = 0^\circ$) and with $\delta = 2^\circ$ and 6° . Two diffraction peaks located at 38.3° and 58.9° can be found and ascribed to $(\bar{4}02)$ and $(\bar{6}03)$ planes of Ga_2O_3 , respectively, suggesting the epitaxial relationship of Ga_2O_3 ($\bar{2}01$)|| Al_2O_3 (0001).

To further examine the crystalline quality of the $\text{Si}:\text{Ga}_2\text{O}_3$ films, XRD phi scans and rocking curve measurements have been carried out. Figure S2 shows the XRD rocking curves of 0.5% $\text{Si}:\text{Ga}_2\text{O}_3$ thin films grown on different substrates, which indicates that the film grown on substrate with 6° miscut angle has a smaller FWHM (1.59°) than that of film grown on substrate without miscut angle ($\delta = 0^\circ$, FWHM = 2.50°). XRD phi scans from $(\bar{4}01)$ skew-symmetric Bragg reflections were performed as shown in Fig. 1(b). Six strong reflection peaks separated by 60° are observed for the films grown on Al_2O_3 substrates without miscut angle, due to its sixfold in-plane rotational symmetry. It is a combination of the twofold in-plane rotational domains of monoclinic Ga_2O_3 and the threefold rotational symmetry of substrates.³⁰ However, for films grown on 2° and 6° miscut substrates, the number of peaks decreased, and only one peak dominated in the phi scan for $\delta = 6^\circ$, indicating that the in-plane domain structures and rotational symmetry are strongly suppressed. This indicates that the films grown on vicinal substrates have preferred growth orientation and the characteristics of step-flow growth mode. This can also be further visualized from the surface morphologies, shown in Fig. 1(c). The film grown on the substrate without miscut angle shows granular structures, while the film grown on $\delta = 6^\circ$ substrate exhibits more regular step-like features. The preferred growth orientation and different morphology on miscut substrates are attributed to the change in growth mechanism guided by the high density of atomic steps on

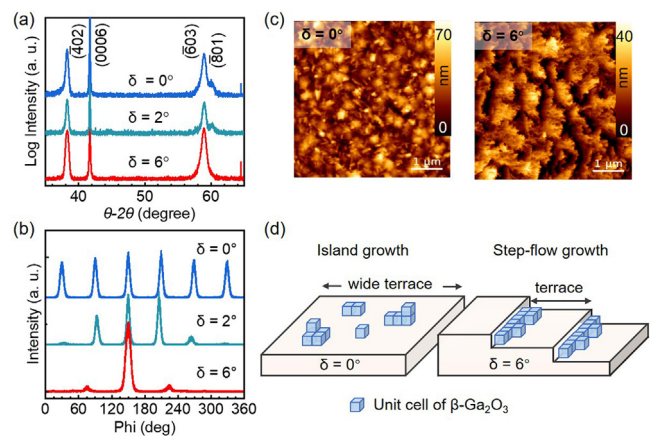


FIG. 1. (a) θ - 2θ XRD patterns of 0.5% Si-doped Ga_2O_3 (0.5% $\text{Si}:\text{Ga}_2\text{O}_3$) films grown on Al_2O_3 (0001) substrates with different miscut angles of 0° , 2° , and 6° toward $[11\bar{2}0]$ direction. (b) Phi-scans of the $(\bar{4}01)$ plane of 0.5% $\text{Si}:\text{Ga}_2\text{O}_3$ thin films. (c) AFM images of 0.5% $\text{Si}:\text{Ga}_2\text{O}_3$ films ($5 \times 5 \mu\text{m}^2$) on 0° and 6° vicinal Al_2O_3 (0001) substrates, respectively. (d) Schematic illustrations of the growth mode of Ga_2O_3 films deposited on Al_2O_3 (left, island growth) and vicinal Al_2O_3 substrate (right, step-flow growth), respectively.

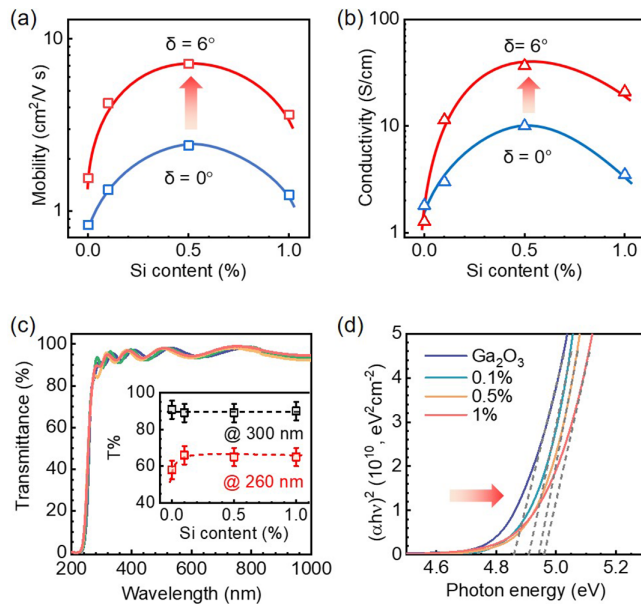


FIG. 2. (a) Hall mobility and (b) conductivity of Si:Ga₂O₃ thin films grown on 0° and 6° miscut Al₂O₃ (0001) substrates as a function of Si doping level. (c) Transmittance spectra and (d) $(\alpha h\nu)^2$ vs $h\nu$ plot of Si:Ga₂O₃ films with different Si content (violet, 0%; green, 0.1%; orange, 0.5%; red, 1%). The inset in (c) shows the transmittance of Si:Ga₂O₃ films at $\lambda = 300$ and 260 nm as a function of Si doping level.

vicinal substrates, as schematically shown in Fig. 1(d). For films grown on the substrate without miscut angle, the substrate surface terrace is wide and there are no preferential sites for Ga adatoms to nucleate, leading to three-dimensional island growth mode. On the other hand, on the vicinal substrates, the surface terrace width became small enough and steps act as the preferential binding sites for Ga adatoms. This suppresses the random nucleation on the surface and promotes step-flow growth mode along the miscut direction. The step growth mode and preferred growth orientation could effectively reduce twin lamellae and grain boundaries, and therefore, improve the electrical properties of the Si:Ga₂O₃ films.³¹

Figures 2(a) and 2(b) show the room temperature Hall mobilities (μ) and conductivities (σ) as a function of Si doping levels for films on

substrates without miscut angle ($\delta = 0^\circ$) and with $\delta = 6^\circ$. The films on $\delta = 6^\circ$ substrates show substantially improved mobility and conductivity compared with films on $\delta = 0^\circ$ substrates. In particular, the 0.5% Si-doped film exhibits the highest conductivity of ~ 37 S·cm⁻¹ and mobility of 7.2 cm² V⁻¹ s⁻¹, which are about three times higher than that of film grown on $\delta = 0^\circ$ substrates. Figure 2(c) presents the optical transmittance of the Si:Ga₂O₃ films in the 200–1000 nm wavelength range, showing that the Si:Ga₂O₃ films possess a high transmittance of over 85% in the ultraviolet region of 260–400 nm. Si doping slightly increases the transmittance of the films in the DUV region [inset of Fig. 2(c)] because of the blueshift of the bandgap caused by doping. The direct optical bandgaps of Si:Ga₂O₃ thin films are extrapolated by the Tauc plot [Fig. 2(d)]. The Tauc relation can be expressed as $(\alpha h\nu)^2 \propto (h\nu - E_g)$, where α is the absorption coefficient and $h\nu$ is photon energy.^{32,33} The bandgaps increase from 4.86 to 4.96 eV with increasing Si doping, due to the filling of the conduction band (CB) by free electrons, i.e., Burstein–Moss effect.³⁴ Table I summarizes the electrical and optical properties of our Ga₂O₃ thin films compared with those reported in previous works. It can be seen that the Si:Ga₂O₃ films grown on vicinal Al₂O₃ substrates exhibit much better conductivity and transparency in the DUV region.

The surface electronic properties of the Si:Ga₂O₃ films are important for transparent electrode application. We used XPS and UPS to further explore the surface electronic structures, band bending and work functions of the grown Si:Ga₂O₃ films. Figures 3(a) and 3(b) show the Ga 2p_{3/2} and valence band (VB) XPS spectra of the Si:Ga₂O₃ films, respectively. As the Si doping level increases from 0% to 0.1%, a shift toward higher binding energies in both Ga 2p_{3/2} and VB maximum (VBM) can be observed, because of the up-movement of the Fermi level (E_F) with the increase in the electron doping. This variation is consistent with the increase in the optical bandgap by the Burstein–Moss effect as mentioned above. A schematic energy diagram for the electronic structure of Ga₂O₃ with Si doping is shown in Fig. 3(c). Based on the free-electron model, the Burstein–Moss shift (ΔBM) can be calculated by $\Delta BM = \frac{h^2 k^2}{8\pi^2 m^*}$, where h is the Planck's constant, m^* is the electron effective mass, and $k = (3n_e \pi^2)^{1/3}$ is the Fermi wave vector, where n_e is carrier concentration.³⁴ Figure 3(d) summarizes the value of ΔBM and the change in optical bandgap (E_{opt}), VBM, and average core level binding energies. The shift values of ΔBM are in agreement with the change in E_{opt} as a function of Si doping because the bottom of the CB is filled with electrons. Nevertheless, for 0.5% and 1% Si-doped films, the shifts of VBM and

TABLE I. Summary of optical and electrical properties of the n -type doped Ga₂O₃ films with different deposition methods from literatures, including transmittance, mobility, and conductivity.

Dopants	Substrate	Method	Transmittance	Mobility (cm ² V ⁻¹ s ⁻¹)	Conductivity (S·cm ⁻¹)	Reference
Si	Al ₂ O ₃	PLD	90% ($\lambda = 300$ nm) 65% ($\lambda = 260$ nm)	7.2	37	This work
Sn	Glass/Al ₂ O ₃	PLD	55% ($\lambda = 248$ nm)	0.44	1	20
Sn	Al ₂ O ₃	PLD	80% ($\lambda = 300$ nm)	...	8.2	22
Si	Al ₂ O ₃	PLD	90% ($\lambda = 300$ nm)	0.1	2	47
Si	Al ₂ O ₃	PLD	90% ($\lambda = 300$ nm)	2.9	11.7	48
Si	Al ₂ O ₃	MOCVD	50% ($\lambda = 280$ nm)	11.8	0.49	49
Si	Fe:Ga ₂ O ₃ (010)	PLD	20% ($\lambda = 280$ nm)	64.5	2323	11

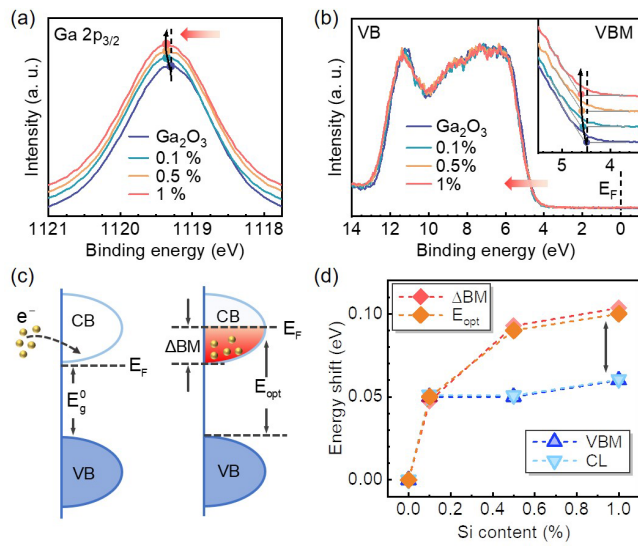


FIG. 3. (a) Ga $2p_{3/2}$ core level and (b) valence-band XPS spectra (inset: valence band maximum edges) for the Si:Ga $_2$ O $_3$ films series. (c) Schematic energy diagram for Si:Ga $_2$ O $_3$ based on free-electron model. (d) Energy shifts of Burstein-Moss (ΔBM), optical bandgap (E_{opt}), VBM, and average of core levels (CL) as a function of Si content.

core levels are smaller than the change in the ΔBM and E_{opt} . This discrepancy can be resolved by considering the XPS is a surface sensitive technique, and there is an upward band bending existing in the surface region of Si:Ga $_2$ O $_3$ films.

We used a model to quantitatively estimate the value of surface band bending (ϕ_{bb}).^{35,36} For Ga $_2$ O $_3$, the Ga $3d$ is located at 16.88 ± 0.05 eV below the VBM (i.e., $\Delta E_{Ga\ 3d-VBM}$, measured by hard x-ray photoelectron spectroscopy in Fig. S3).^{37,38} Therefore, the amount of surface band bending can be calculated by $\phi_{bb} = E_g^0 + \Delta BM + \Delta E_{Ga\ 3d-VBM} - E_{Ga\ 3d}$, where $E_{Ga\ 3d}$ is the binding energy of Ga $3d$. The calculated values of ϕ_{bb} , work functions (ϕ), and the measured VBM are summarized in Table II. There is a 0.35 eV upward band bending at the surface region of undoped Ga $_2$ O $_3$, and the value of band bending slightly increases with the increase in Si doping [a 0.39 eV upward band bending for 1% Si:Ga $_2$ O $_3$, as shown in Fig. 4(a)]. The upward surface band bending in Ga $_2$ O $_3$ is very different from the traditional transparent oxide semiconductors, i.e., In $_2$ O $_3$ and SnO $_2$ show downward surface band bending (electron accumulation layer).^{39–41} This is mainly due to the fact that the charge neutrality

TABLE II. Summary the values of the surface band bending, work functions, and VBM for Si-doped Ga $_2$ O $_3$ thin films.

Si doping level (%)	Surface band bending (ϕ_{bb} , eV)	Work function (ϕ , eV)	VBM (eV)
0	0.35	3.22	4.53
0.1	0.36	3.31	4.58
0.5	0.39	3.44	4.58
1	0.39	3.45	4.59

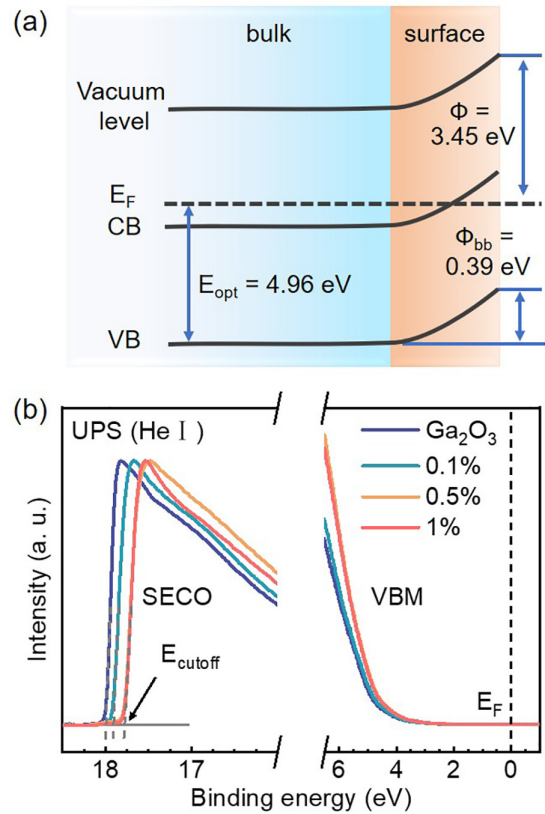


FIG. 4. (a) Schematic energy diagram of the band bending at the surface of 1% Si:Ga $_2$ O $_3$ thin film (ϕ , work function; ϕ_{bb} , surface band bending). (b) The UPS spectra (He I, $h\nu = 21.22$ eV) for Si:Ga $_2$ O $_3$ thin films.

level (CNL) of Ga $_2$ O $_3$ is located at 0.6 eV below the CBM derived by Ga $4s$ orbital, and a depletion layer will occur on the surface to compensate for negatively charged surface states.³⁵ With the increase in carrier concentration, the upward band bending increases, because the Fermi level moves further away from the CNL.

We used UPS to measure the work functions of the grown Si:Ga $_2$ O $_3$ films. Figure 4(b) shows the secondary electron cutoff (SECO) and the VBM of the films measured by UPS. Based on $\phi = h\nu - (E_{cutoff} - E_F)$, the work functions are determined to be 3.22 eV for undoped Ga $_2$ O $_3$, 3.31 eV for 0.1%, 3.44 eV for 0.5%, and 3.45 eV for 1% Si:Ga $_2$ O $_3$ films. The work functions of Si:Ga $_2$ O $_3$ films are much smaller than that of In $_2$ O $_3$ and SnO $_2$ (4.2–5.0 eV).^{42–45} A low work function conductive cathode is highly needed in OLEDs to promote the electron injection into the lowest unoccupied molecular orbital (LUMO) of the organic semiconductor and then realize high-performance photoelectric devices.⁴⁶ The DUV transparent Si:Ga $_2$ O $_3$ thin films with conductivity and low work function have the potential to be used in OLEDs and other optoelectronic devices.

In summary, we fabricated highly conductive and DUV transparent Si:Ga $_2$ O $_3$ thin films on vicinal Al $_2$ O $_3$ (0001) substrates. It is found that the growth model, crystalline quality, electrical properties, and surface morphologies of Si:Ga $_2$ O $_3$ thin films are closely related to the miscut angle. 0.5% Si-doped film grown on the 6° miscut substrate

shows the highest conductivity of $37 \text{ S}\cdot\text{cm}^{-1}$ and attractive average transparency of 85% in 260–400 nm wavelength. An upward band bending was found at the surface region of Si:Ga₂O₃ films, which is in stark contrast to the downward surface band bending found for other oxide semiconductors, such as In₂O₃ and SnO₂. The upward band bending can be explained by the low charge neutral level in Ga₂O₃. Furthermore, the Si:Ga₂O₃ films have low work functions of $\sim 3.3 \text{ eV}$, making them promising as efficient electron injection materials. The results and the understanding of surface electronic properties for Si:Ga₂O₃ films would be a guideline for developing advanced DUV transparent electrodes with the characteristics of high DUV transparency, conductivity, and low work functions.

See the [supplementary material](#) for characterizations of β -Ga₂O₃ thin films, such as θ -2 θ XRD patterns, rocking curves, and hard x-ray photoelectron spectroscopy.

This work was supported by the National Natural Science Foundation of China (Grant No. 22275154) and the Shenzhen Science and Technology Program (Grant No. JCYJ20220530143016036).

AUTHOR DECLARATIONS

Conflict of Interest

The authors have no conflicts to disclose.

Author Contributions

Zhenni Yang: Data curation (lead); Writing – original draft (lead). **Xiangyu Xu:** Formal analysis (equal); Validation (equal). **Yan Wang:** Data curation (equal); Investigation (equal). **Siliang Kuang:** Investigation (equal); Methodology (equal). **Duan yang Chen:** Methodology (equal). **Hong Ji Qi:** Conceptualization (equal); Writing – review & editing (equal). **Kelvin H. L. Zhang:** Conceptualization (lead); Writing – review & editing (lead).

DATA AVAILABILITY

The data that support the findings of this study are available from the corresponding authors upon reasonable request.

REFERENCES

- H. Hosono, *Thin Solid Films* **515**, 6000 (2007).
- H. Hirayama, N. Maeda, S. Fujikawa, S. Toyoda, and N. Kamata, *Jpn. J. Appl. Phys., Part 1* **53**, 100209 (2014).
- M. Wei, L. Gong, D. D. Liang, H. J. Cho, and H. Ohta, *Adv. Electron. Mater.* **6**, 2000100 (2020).
- Y. Nagashima, M. Fukumoto, M. Tsuchii, Y. Sugisawa, D. Sekiba, T. Hasegawa, and Y. Hirose, *Chem. Mater.* **34**, 10842 (2022).
- S. Liu, W. Luo, D. Li, Y. Yuan, W. Tong, J. Kang, Y. Wang, D. Li, X. Rong, T. Wang, Z. Chen, Y. Li, H. Wang, W. Wang, J. Hoo, L. Yan, S. Guo, B. Shen, Z. Cong, and X. Wang, *Adv. Funct. Mater.* **31**, 2008452 (2021).
- G. Matafonova and V. Batoev, *Water Res.* **132**, 177 (2018).
- M. Kneissl, T.-Y. Seong, J. Han, and H. Amano, *Nat. Photonics* **13**, 233 (2019).
- H.-D. Kim, H.-M. An, K. H. Kim, S. J. Kim, C. S. Kim, J. Cho, E. F. Schubert, and T. G. Kim, *Adv. Funct. Mater.* **24**, 1575 (2014).
- J. Zhang, J. Shi, D.-C. Qi, L. Chen, and K. H. L. Zhang, *APL Mater.* **8**, 020906 (2020).
- Z. Feng, A. F. M. Anhar Uddin Bhuiyan, M. R. Karim, and H. Zhao, *Appl. Phys. Lett.* **114**, 250601 (2019).
- H. M. Jeon, K. D. Leedy, D. C. Look, C. S. Chang, D. A. Muller, S. C. Badescu, V. Vasilyev, J. L. Brown, A. J. Green, and K. D. Chabak, *APL Mater.* **9**, 101105 (2021).
- J. Zhang, J. Willis, Z. Yang, Z. Sheng, L.-S. Wang, T.-L. Lee, L. Chen, D. O. Scanlon, and K. H. L. Zhang, *Cell Rep. Sci.* **3**, 100801 (2022).
- J. Zhang, J. Willis, Z. Yang, Z. Sheng, L.-S. Wang, T.-L. Lee, L. Chen, D. O. Scanlon, and K. H. L. Zhang, *Phys. Rev. B* **106**, 205305 (2022).
- K. N. Heinselman, D. Haven, A. Zakutayev, and S. B. Reese, *Cryst. Growth Des.* **22**, 4854 (2022).
- Z. Guo, A. Verma, X. Wu, F. Sun, A. Hickman, T. Masui, A. Kuramata, M. Higashiwaki, D. Jena, and T. Luo, *Appl. Phys. Lett.* **106**, 111909 (2015).
- T.-C. Hsu, Y.-T. Teng, Y.-W. Yeh, X. Fan, K.-H. Chu, S.-H. Lin, K.-K. Yeh, P.-T. Lee, Y. Lin, Z. Chen, T. Wu, and H.-C. Kuo, *Photonics* **8**, 196 (2021).
- Y. Nagasawa and A. Hirano, *Appl. Sci.* **8**, 1264 (2018).
- Y. Chen, H. Liang, X. Xia, P. Tao, R. Shen, Y. Liu, Y. Feng, Y. Zheng, X. Li, and G. Du, *J. Mater. Sci.* **26**, 3231 (2015).
- Y. Li, X. Xiu, W. Xu, L. Zhang, Z. Xie, T. Tao, P. Chen, B. Liu, R. Zhang, and Y. Zheng, *J. Phys. D* **54**, 014003 (2021).
- M. Orita, H. Ohta, M. Hirano, and H. Hosono, *Appl. Phys. Lett.* **77**, 4166 (2000).
- F. Zhang, M. Arita, X. Wang, Z. Chen, K. Saito, T. Tanaka, M. Nishio, T. Motoooka, and Q. Guo, *Appl. Phys. Lett.* **109**, 102105 (2016).
- M. Orita, H. Hiramatsu, H. Ohta, M. Hirano, and H. Hosono, *Thin Solid Films* **411**, 134 (2002).
- S. Rafique, L. Han, A. T. Neal, S. Mou, J. Boeckl, and H. Zhao, *Phys. Status Solidi A* **215**, 1700467 (2018).
- S. Bin Anooz, R. Grüneberg, C. Wouters, R. Schewski, M. Albrecht, A. Fiedler, K. Irmscher, Z. Galazka, W. Miller, G. Wagner, J. Schwarzkopf, and A. Popp, *Appl. Phys. Lett.* **116**, 182106 (2020).
- P. Mazzolini, A. Falkenstein, Z. Galazka, M. Martin, and O. Bierwagen, *Appl. Phys. Lett.* **117**, 222105 (2020).
- R. Schewski, K. Lion, A. Fiedler, C. Wouters, A. Popp, S. V. Levchenko, T. Schulz, M. Schmidbauer, S. Bin Anooz, R. Grüneberg, Z. Galazka, G. Wagner, K. Irmscher, M. Scheffler, C. Draxl, and M. Albrecht, *APL Mater.* **7**, 022515 (2019).
- H. Li, Y. Wang, J. Cao, Y. Qi, J. Yu, Z. Dong, J. Shen, S. Li, Y. Jiang, W. Tang, and Z. Wu, *J. Alloys Compd.* **877**, 160143 (2021).
- H. Sun, S. Mitra, R. C. Subedi, Y. Zhang, W. Guo, J. Ye, M. K. Shakfa, T. K. Ng, B. S. Ooi, I. S. Roqan, Z. Zhang, J. Dai, C. Chen, and S. Long, *Adv. Funct. Mater.* **29**, 1905445 (2019).
- Y. J. Ma, X. D. Zhang, B. Y. Feng, W. B. Tang, T. W. Chen, H. Qian, L. Zhang, X. Zhou, X. Wei, K. Xu, H. Q. Fu, and B. S. Zhang, *Vacuum* **198**, 110886 (2022).
- V. Gottschalch, K. Mergenthaler, G. Wagner, J. Bauer, H. Paetzelt, C. Sturm, and U. Teschner, *Phys. Status Solidi A* **206**, 243 (2009).
- R. Schewski, M. Baldini, K. Irmscher, A. Fiedler, T. Markurt, B. Neuschulz, T. Remmele, T. Schulz, G. Wagner, Z. Galazka, and M. Albrecht, *J. Appl. Phys.* **120**, 225308 (2016).
- D. L. Wood and J. Tauc, *Phys. Rev. B* **5**, 3144 (1972).
- E. A. Davis and N. F. Mott, *Philos. Mag.* **22**, 0903 (1970).
- A. Walsh, J. L. F. Da Silva, and S.-H. Wei, *Phys. Rev. B* **78**, 075211 (2008).
- J. E. N. Swallow, J. B. Varley, L. A. H. Jones, J. T. Gibbon, L. F. J. Piper, V. R. Dhanak, and T. D. Veal, *APL Mater.* **7**, 022528 (2019).
- Y. Imazeki, M. Sato, T. Takeda, M. Kobayashi, S. Yamamoto, I. Matsuda, J. Yoshinobu, M. Sugiyama, and Y. Nakano, *J. Phys. Chem. C* **125**, 9011 (2021).
- S. Ghosh, M. Baral, R. Kamparath, S. D. Singh, and T. Ganguli, *Appl. Phys. Lett.* **115**, 251603 (2019).
- H. Sun, C. G. Torres Castanedo, K. Liu, K.-H. Li, W. Guo, R. Lin, X. Liu, J. Li, and X. Li, *Appl. Phys. Lett.* **111**, 162105 (2017).
- S. K. Vasheghani Farahani, T. D. Veal, J. J. Mudd, D. O. Scanlon, G. W. Watson, O. Bierwagen, M. E. White, J. S. Speck, and C. F. McConville, *Phys. Rev. B* **90**, 155413 (2014).
- K. H. Zhang, R. G. Egdell, F. Offi, S. Iacobucci, L. Petaccia, S. Gorovikov, and P. D. King, *Phys. Rev. Lett.* **110**, 056803 (2013).
- P. D. C. King, T. D. Veal, F. Fuchs, C. Y. Wang, D. J. Payne, A. Bourlange, H. Zhang, G. R. Bell, V. Cimalla, O. Ambacher, R. G. Egdell, F. Bechstedt, and C. F. McConville, *Phys. Rev. B* **79**, 205211 (2009).

- ⁴²Y. Sato, T. Ashida, N. Oka, and Y. Shigesato, *Appl. Phys. Express* **3**, 061101 (2010).
- ⁴³C. A. Pan and T. P. Ma, *Appl. Phys. Lett.* **37**, 714 (1980).
- ⁴⁴K. Rachut, C. Körber, J. Brötz, and A. Klein, *Phys. Status Solidi A* **211**, 1997 (2014).
- ⁴⁵G. C. J. Szuber, R. Larciprete, and B. Adamowicz, *Sens. Actuators, B* **70**, 177 (2000).
- ⁴⁶Y. Zhou, C. Fuentes-Hernandez, J. Shim, J. Meyer, A. J. Giordano, H. Li, P. Winget, T. Papadopoulos, H. Cheun, J. Kim, M. Fenoll, A. Dindar, W. Haske, E. Najafabadi, T. M. Khan, H. Sojoudi, S. Barlow, S. Graham, J.-L. Brédas, S. R. Marder, A. Kahn, and B. Kippelen, *Science* **336**, 327 (2012).
- ⁴⁷F. Zhang, K. Saito, T. Tanaka, M. Nishio, and Q. Guo, *J. Mater. Sci.* **26**, 9624 (2015).
- ⁴⁸S. Khartsev, N. Nordell, M. Hammar, J. Purans, and A. Hallén, *Phys. Status Solidi B* **258**, 2000362 (2021).
- ⁴⁹Y. Zhu, D. Zhang, W. Zheng, and F. Huang, *J. Phys. Chem. C* **124**, 16722 (2020).